Available online at www.sciencedirect.com
SCIENCE DIRECT
Journal of Volcanology and Geothermal Research 153 (2006) 64–79
Journal of volcanology and geothermal research
www.elsevier.com/locate/jvolgeores

Seismic characteristics of variable convection at Erta ‘Ale lava lake, Ethiopia

Joshua Jones [a,*], Roberto Carniel [b], Andrew J.L. Harris [c], Steve Malone [a]

[a] Department of Earth and Space Sciences, University of Washington, Seattle, Washington, Box 351310, Seattle, WA 98195-1310, USA
[b] Dipartimento di Georisorse e Territorio, Università di Udine, Via Cotonificio, 114; 33100 Udine, Italy
[c] HIGP/SOEST, University of Hawai‘i, Honolulu, Hawai‘i, USA

Received 1 June 2004; accepted 18 August 2005
Available online 20 January 2006

Abstract

The active summit lava lake of Erta ‘Ale volcano, Ethiopia, offers a unique opportunity to study magma convection. In February 2002, we collected a multiparametric set of seismic, thermal and video data. These data indicate that the lake cycled between periods characterized by low (0.01–0.08 m s^{-1}) and high (0.1–0.4 m s^{-1}) convection rates, typically lasting tens to hundreds of minutes. Three seismometers placed around the active crater recorded continuous tremor with a dominant frequency of 2 Hz, and energy at frequencies from 0.8 to 12 Hz. Here, we characterize the seismic signature of each regime by its spectral content, wavefield polarization, and tremor source location. For both regimes, the wavefield is mostly rectilinear. Azimuths and incidence angles are consistent with P waves originating in one of two locations: the north edge of the active lava lake, or a region 100–150 m ENE of the lava lake. Because both regimes are dominated by a low frequency, rectilinearly polarized wavefield, we investigate the source location using a method that solves for location and isotropic source power by a weighted least-squares amplitude-based inversion of seismic data. We find that tremor source regions are unique to each convective regime, although some location overlap exists when tremor is located in short time windows. Wavefield composition suggests that the convective phases may share a common source process, but their differing locations indicate that either the source region is non-stationary, or a second source skews the location during the high convective phase. Tremor polarization and location suggests that the low-frequency tremor is caused by bubble coalescence and bursting in a conduit whose surface is the lava lake. The higher frequency signal associated with the high convective regime is associated with a scattered, more complex wavefield superimposed on the low-frequency background tremor, caused by bubble bursting and cracking of cooled crust at the lava lake surface.

Keywords: lava lakes; Erta Ale; convection; seismic; thermal; volcanic tremor; polarization analysis; seismic source location

1. Introduction

Erta ‘Ale volcano (13.60°N, 40.67°E, Fig. 1) is a basaltic shield volcano in the Danakil depression of northeast Ethiopia, with a summit 613 m asl (Barberi and Varet, 1970). Its 1600×700 m^2 summit caldera features two pit craters. Since the early 1970s, when access was restricted due to political conditions, the southern crater has hosted an active lava lake (Oppenheimer and Francis, 1998). However, active lava lakes have been continuously present at Erta ‘Ale since at least 1967, and possibly since 1906 (Dainelli and Marinelli, 1907; Martini, 1969).

* Corresponding author. Tel.: +1 206 543 6626; fax: +1 206 543 0489.
E-mail address: josh@ess.washington.edu (J. Jones).

0377-0273/$ - see front matter © 2005 Elsevier B.V. All rights reserved.
doi:10.1016/j.jvolgeores.2005.08.004

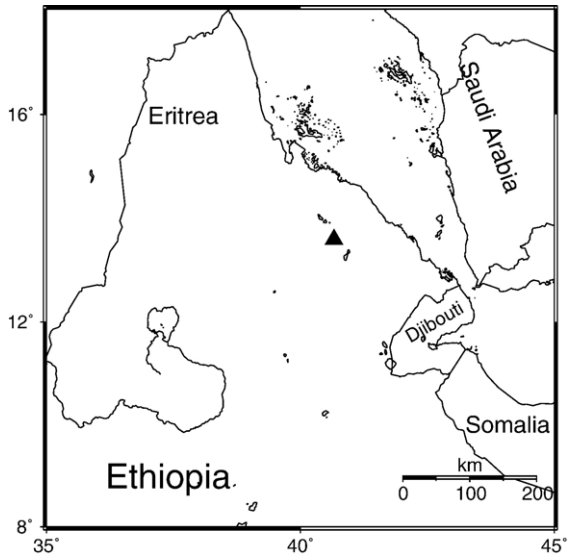

Fig. 1. Map showing the location of Erta ‘Ale, Ethiopia. Black triangle indicates location of the Erta ‘Ale summit caldera.

Active lava lakes can be considered the exposed upper surface of a convecting magma column, and often indicate a relatively simple conduit (Swanson et al., 1979; Harris et al., 1999). In addition, surface convective features at active lava lakes resemble global plate tectonics (Duffield, 1972) and may be used as a proxy for shallow convective motions (Harris et al., 2005). Long-lived lava lakes require well-developed magma circulation between the reservoir, conduit, and lava lake itself (Francis et al., 1993; Tazieff, 1994; Oppenheimer and Francis, 1998). Magma circulation is necessary to insure summit lava lake longevity, and can persist for tens to hundreds of years (Harris et al., 1999). Thus, active summit lava lakes can provide quasi-direct, long-term, continuous observations of magma system circulation and associated physical parameters, such as volcanic tremor, deformation, heat flux, and gas release (e.g. Le Guern, 1987; Hamaguchi et al., 1992; Kaminuma, 1994; Kyle et al., 1994; Oppenheimer and Francis, 1997; Amelung et al., 2000).

Persistent, active summit lava lakes are relatively uncommon, and have been documented only at a handful of volcanoes around the world. Examples include Ambrym, Vanuatu, since 1996, barring a brief period when a large regional earthquake triggered rock falls, covering the lava lake (Carniel et al., 2003); Nyamuragira, D.R. Congo, from 1921 to 1938 (Hantke, 1939); Nyiragongo, D.R. Congo, for at least 50 yrs, through 1977 (Tazieff, 1977); Kilauea, Hawai‘i, United States, periodically through 1924 (Macdonald et al., 1970), and periodically during recent eruptive activity (e.g. Duffield, 1972; Tilling, 1987); Masaya, Nicaragua, periodically in the 1980s and 1990s (Rymer et al., 1998); Villarrica, Chile (Witter, 2003); Erebus, Antarctica (Kyle, 1994; Aster et al., 2004); and Erta ‘Ale, Ethiopia, since at least 1967, and possibly since 1906 (Dainelli and Marinelli, 1907; Martini, 1969). Finally, a lava lake has recently been discovered on Saunders Island, S. Sandwich Islands (Lachlan-Cope et al., 2001), at which activity persists through 2004 (Patrick et al., 2005).

Here we take advantage of the persistent activity at the Erta ‘Ale lava lake to complete a multiparametric study, involving simultaneous collection of seismic, thermal and video data, to better understand the dynamic of the shallow system that feeds this lake. The concept of multiparametric studies (e.g. McNutt et al., 2000) has developed considerably over the last few years, and was greatly expanded upon by the MULTIMO project: multiparametric data sets are now incorporated into modeling work (Neuberg et al., 2006-this issue), used in risk evaluation for occurrence of given eruptive scenarios (Aspinall et al., 2003, 2006-this issue), and are increasingly available via efficient data delivery systems (e.g. Carniel et al., 2006-this issue).

For lava lake systems, considerable advances in our understanding of lava lake processes and conduit dynamics have been possible from such multiparametric approaches. Tilling (1987), for example, used tilt and lava lake level data during the 1972–1974 Mauna Ulu eruption, Kilauea, to show a clear linkage between the summit reservoir and a lava lake system on the volcano flank. Barker et al. (2003) used deformation, lake level and seismic data for lava lakes in Pu ‘u ‘O ‘o to reveal and understand pond filling and drainage due to gas pistoning. Erebus is another particularly well-monitored system (e.g. Kyle, 1994), where, for example, gas flux and seismic data revealed a marked change in activity during 1984 (Kaminuma, 1994; Kyle et al., 1994).

Thus, motivated by the persistence of the Erta ‘Ale lava lake, and the success of multiparametric campaigns at other volcanoes, a brief survey at Erta ‘Ale volcano, Afar, Ethiopia, incorporated simultaneous seismic, thermal, and video data acquisition (Alean et al., 2005; Harris et al., 2005) to understand the effects of convection on activity within the lake. In this study, we use a combined thermal and seismic data set, constrained by video observations. In Harris et al. (2005) we concentrated on an interpretation of the thermal signal, supported by the seismic data, to track convection processes in the lake. Here, we focus on the seismic signal to search for signals that may be directly associated with variable rates of lava lake convection indicated by the thermal data.

2. Data

Our February 2002 experiment involved simultaneous acquisition of seismic, thermal, and video data. Three seismic stations were installed: a Lennartz MarsLite station, a Guralp CMG-40 broadband seismometer; and a Mark Products L-22 seismometer. All station locations are shown in Fig. 2. Details on sensor type, sampling frequencies, and station recording times are given in Table 1. All stations used a preamplification gain of unity.

The thermal section of the experiment is described in detail in Harris et al. (2005) and involved a single Omega thermal infrared thermometer. This was installed on the rim of the southern pit, where the 1° field of view was aimed centrally in the active lava lake. This instrument provides temperatures in the range −18 to 1370 °C integrated over a 1° field of view (FOV). The infrared thermometer acquired three separate data sets over almost identical FOVs on 17, 18 and 19 February, respectively, sampling at 0.33 Hz, with a data set duration of approximately 24 h. In addition, video data was acquired with digital video cameras from the crater rim. All data logger, computer, and video camera clocks were synchronized using a Garmin handheld GPS unit, with estimated accuracy of 1 s. All times given in this paper are GMT. All coordinates use the WGS 72 datum.

The most notable feature of the seismic data is that all three seismic stations recorded continuous volcanic tremor with a main spectral peak around $f=2$ Hz (Fig. 3). This spectral peak is too broad for the tremor to be considered monochromatic, but is persistent and stable. In addition to the broad 2 Hz spectral peak, the energy of the band of 6–12 Hz spectral band changes on time scales of one to several hours, where significant energy is observed in bursts lasting a few minutes to several hours (Fig. 3b). Tremor amplitude is relatively constant, though, and does not vary by more than a factor of 2, averaging around 5×10^{-6} m/s (Fig. 3a).

The continuous tremor is the only obvious signal with a possible local origin. There were no large explosions during the 5-day experiment. No teleseisms, very long period events, large rock falls, or volcano–tectonic earthquakes were recorded. One audible explosion occurred, around 09:30 AM on 15 February 2002 (GMT), but produced no discrete seismic signals discernible above the continuous tremor. While fountaining episodes were recorded by video and thermal data, these were extremely small, on the order of 2–5 m in height, persisted for only a few seconds to a few minutes each, and produced no seismic signal which can be unambiguously associated with the fountaining itself.

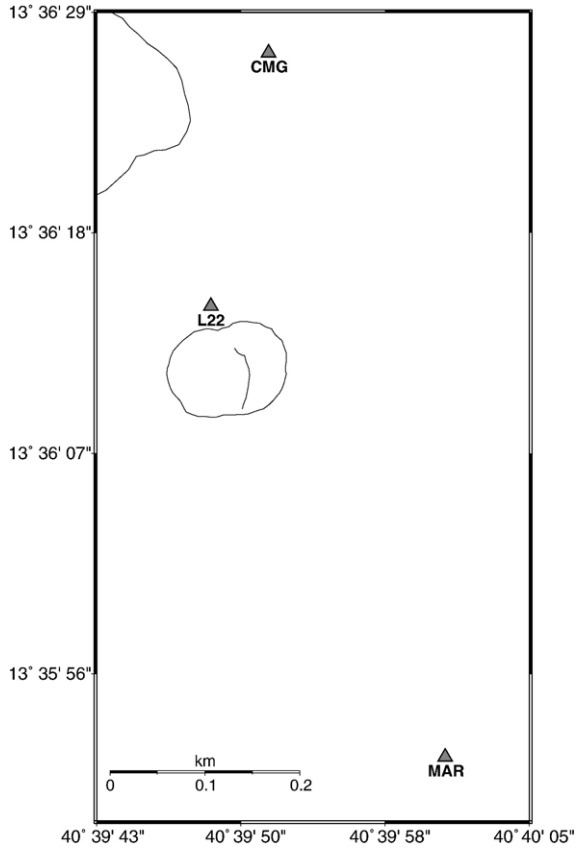

Fig. 2. Instrumentation map showing the seismic instruments used in the 2002 survey, and position of active summit crater. Triangles represent seismic stations. Active crater is indicated with a solid line; the lava lake occupied approximately the western half of the active crater. Station naming convention is fully described in the text.

3. Identification of variable convective regimes

Thermal and seismic data, together with visual observations and video footage, all suggest that convection at the lava lake is not constant (Alean et al., 2005; Harris et al., 2005, Fig. 3a). Instead, during the February 2002 experiment, lava lake convection was found to cycle between two convective regimes, characterized by high and low velocities, respectively (Harris et al., 2005). During the low convective phase, surface crust moves at velocities of 0.01–0.08 m s^{-1}m s^{-1}, while the high convective phase is characterized by crust velocities of 0.1–0.4 m s^{-1}. The lava lake cycles between regimes over periods of tens to hundreds of minutes, typically 50–220 min. Characteristics of these convective periods are discussed in detail in Harris et al.

Table 1
Detailed seismic station information

Station	Latitude	Longitude	Elevation (m asl)	Sensor type	f_0 (Hz)	Install date (mm/dd hh:mm:ss)	Deinstall date (mm/dd hh:mm:ss)
CMG	13.60745	40.66438	575	CMG-40T	0.33	02/14 19:28:32	02/17 06:09:22
L22	13.60400	40.66346	575	L22	2.0	02/15 14:33:16	02/19 06:23:39
MAR	13.59787	40.66683	511	LE-3D	0.2	02/15 09:05:44	02/20 04:25:12

Times are GMT.

(2005). Following the reasoning of Harris et al. (2005), if we assume that the thin, cooled surface crust represents the exposed surface of a convecting layer, then the velocity of the crust can serve as a proxy for convection rate. Thus, we find that the rate of convection increases by over a factor of three during the transition from low to high convective regimes.

As in Harris et al. (2005), we can examine these variable convective regimes by computing spectrograms of seismic and thermal data (Fig. 3b). Seismic spectrograms illustrate the frequency content of the tremor, while thermal spectrograms show changes in the temperature of exposed magma. Here, vigorous periods are characterized by high-frequency changes in thermal energy, up to 0.04 Hz. The physical interpretation of this higher frequency thermal energy is that rapidly moving crusts and/or smaller plates expose cracks (thermal spikes) at a higher rate (Harris et al., 2005). During sluggish activity periods, high frequencies are absent, indicating that temperatures at the lava lake surface are relatively constant. Physically, less vigorous convection means that fewer cracks expose fresh, hot magma to the radiometer FOV and thus reduce the frequency with which thermal spikes occur in the time series.

The seismic spectrograms also show more high-frequency (5–12 Hz) energy during the high convective phase (Fig. 3b). During the low convective regime, the high frequency component of the signal is largely absent. In the first thermal data set, beginning ~08:00 AM on February 17, vigorous activity periods appear in both data sets, showing increased high-frequency seismic energy ($f>6$ Hz) and non-DC ($f>0$ Hz) thermal energy (Fig. 3b). This correspondence between seismic spectrograms, thermal spectrograms, and video observations of changing convective regimes, suggests that the source of Erta ‘Ale’s continuous tremor relates directly to convection in the lava lake.

Because convection in the lava lake appears to influence tremor, it is natural to ask what other properties of the volcanic tremor change with the transition from one convective regime to another. It is also natural to ask if these properties change in some characteristic way that provides clues about possible tremor source processes. Understanding variability in the continuous tremor greatly increases our understanding of the process responsible for generating these signals. Therefore, we take the following approach. First, we examine the wavefield polarization for each convective regime, using the method of Jurkevics (1988), in order to determine the wavefield composition. Second, we attempt to locate samples of continuous tremor from each convective regime, using methods derived from techniques introduced by Gottschämmer and Surono (2000). In particular, we look for characteristic changes in location and polarization that could relate to a possible changing tremor source process.

4. Data selection and preprocessing

Problems with the Reftek SCSI disk severely limit the amount of data available from station L22, which is necessary to insure that the two-variable problem of determining tremor epicenter remains overdetermined. Additionally, because of the station’s proximity to the lava lake, if tremor originates within or near the lava lake, this station will be closest to the source, and therefore provides the most meaningful information about the source process. We therefore limit detailed polarization analysis to station L22, which, in turn, limits our data selection. Because the spectral properties of each convective phase are consistent with successive periods of the same convective phase, however (Fig. 3b), such a limitation should not alter the results.

Prior to analysis, the frequency response of the L22 and CMG-40T sensors were deconvolved from their respective seismic data, and convolved with the response of the LE-3D seismometer ($f_0=0.2$ Hz). In this way, the frequency content of all stations is uniform. Because Fig. 3b suggests that most meaningful seismic energy falls between 0.8 and 12 Hz, this insures that the frequency response of all instruments, in the region of interest, is identical.

5. Polarization analysis

The method of Jurkevics (1988) determines the polarization ellipse by solving the eigenproblem for the covariance matrix of continuous seismic data, which provides a measure of rectilinearity and planarity. The (body wave) azimuth and incidence angle can be estimated from the orientation of the eigenvector associat-

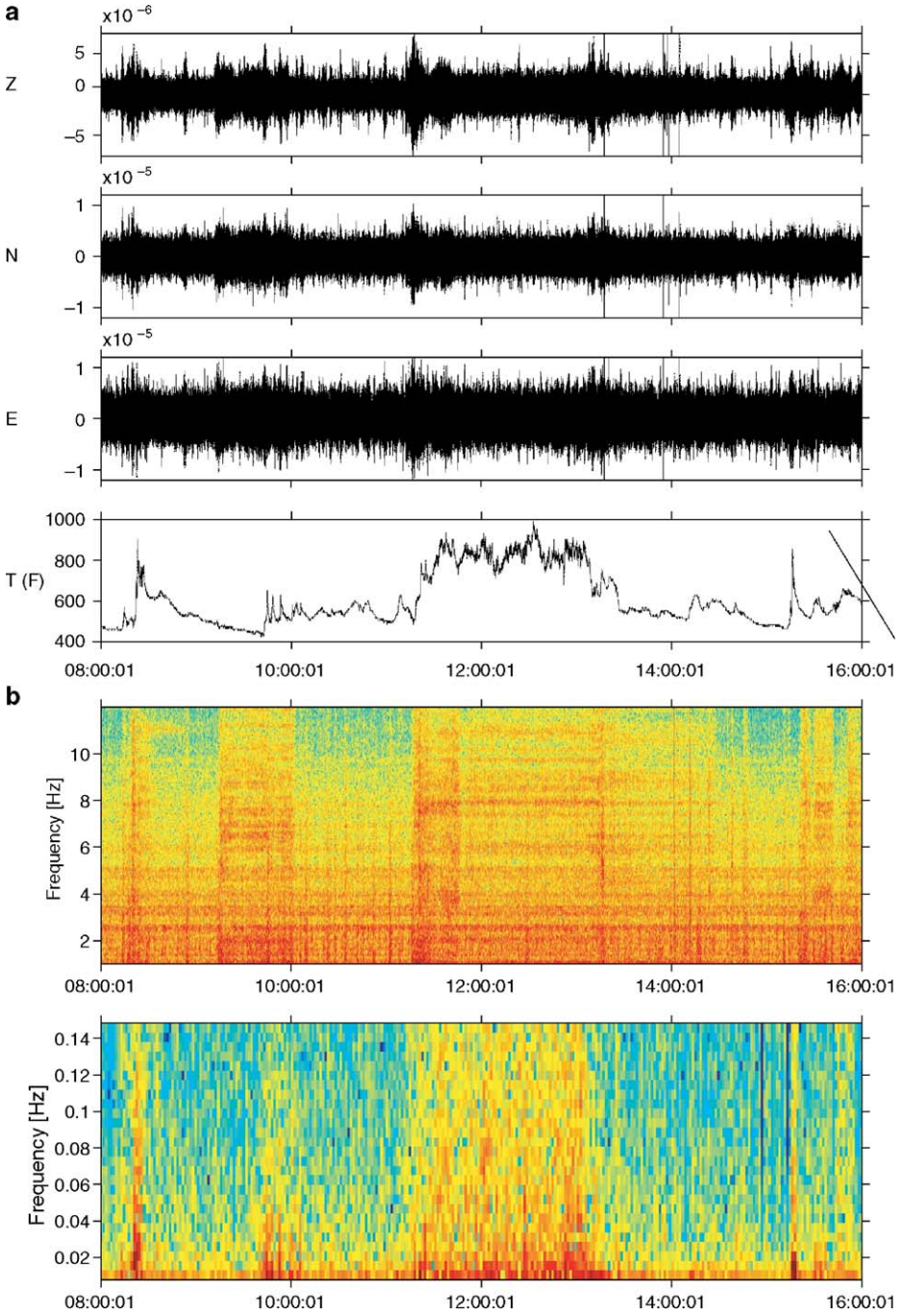

Fig. 3. Raw data and spectrograms. Shown is an 8-h period beginning 17 February 2002, 08:00 GMT. (a) Raw data. Seismic data are three component data from station MAR, sampled at 62.5 Hz. Thermal data are from the radiometer (OME), sampled at 0.33 Hz. Periods of high temperatures correspond to the high convective regime. Periods of low temperatures correspond to the low convective regime. (b) Seismic and thermal spectrograms. Colors are contoured with decibel scaling. Scaling on spectrograms is normalized.

ed with the largest eigenvalue. Therefore, diagonalizing the covariance matrix in moving, non-overlapping time windows creates a time series for each of these four wavefield parameters, with which we analyze the temporal behavior of wavefield polarization. As a stationary source should provide consistent values, the time series generated by this method provide a quantitative estimate of the tremor's quasi-stationarity.

Because we observe that tremor spectral content depends on the convective regime, we begin with polarization analysis of a data segment from station L22, approx. 3-h 45-min long, beginning 05:01 AM on 19 February 2002. The chosen time window includes sample data from each convective regime, and is the largest available time window at the nearest station to the lava lake. Therefore, assuming the tremor source is generated in or near the lava lake, this station's data is least affected by scattering. To insure enough samples for meaningful statistical analysis of both the chosen data segment, and shorter data segments when all three stations were operational, polarization is computed in non-overlapping 20-s segments. However, we find that this analysis produces consistent results for any longer segment length.

Results of this analysis are shown in Fig. 4. We observe immediately that polarization over the frequency range 0.8–12 Hz does not change between the two convective regimes. However, increased high-frequency energy during the high convective phase remains small compared to the energy between 1 and 4.5 Hz, so changes in high-frequency energy have a negligible effect on polarization. Therefore, we examine polarization in greater detail using four narrow, overlapping frequency bands: 0.8–2 Hz, 1.5–4 Hz, 3.5–6 Hz, and 5.5–12 Hz.

The polarization of each frequency band appears in Fig. 5. At low and middle frequencies (Fig. 5a–c), the wavefield shows no significant change in any calculated quantity. For example, in the range of 1.5–4 Hz, azimuth and incidence angle have 1σ uncertainties of 5.4° and 3.3°, respectively, while rectilinearity and planarity have 1σ uncertainties of 0.032 and 0.018. This result, suggested by Fig. 4, indicates that the polarization of the low-frequency energy does not change substantially between the different convective regimes. However, we note distinct changes at frequencies over 5.5 Hz (Fig. 5d): the time series of azimuths becomes less stable during the high convective regime, and even less during the second low convective regime. Incidence angles decrease, but are more stable during the higher convective phase. Thus, polarization of the high-frequency wavefield suggests that tremor source location changes, tremor source mechanism changes, or an additional, high-frequency tremor source appears during the higher convective phase.

Polarization analysis also yields clues about the tremor source mechanism. For both convective regimes, at frequencies under 6 Hz, the station nearest to the lava lake records waves with mostly rectilinear polarization (Fig. 5a–c). However, accounting for polarization's 180° ambiguity, these waves either point toward the edge of the lava lake, or toward a source ENE of the lava lake. Additionally, if the tremor source is near the lava lake, stations CMG and MAR are far enough away that scattering could affect polarization analysis. Thus, this result does not necessarily constrain the position of the tremor source.

To help clarify this ambiguity, polarization is computed for the same time window at station MAR. From Fig. 6, it is clear that body wave azimuths and incidence angles show some scattering; additionally, the wavefield rectilinearity takes somewhat lower values of 0.71–0.83, but still suggests a high degree of rectilinearity. Further, the body wave azimuths favors a tremor source region 100–200 m ENE of the lava lake, a result consistent with the wavefield polarization at station L22 (Fig. 4). Thus, while azimuth and incidence at station L22 suggest tremor could be generated by degassing or magma circulation at the lava lake's edge, the wavefield polarization at station MAR casts some doubt on any such conclusion.

Assuming that this inferred tremor source region is correct, i.e. that the tremor source is 150–250 m ENE of the lava lake, radial polarization provides an important clue about the possible tremor source mechanism. At distances of only 150–250 m to station L22 (cf. Fig. 2), and with assumed phase velocities of 2–5 km/s, this station is within one wavelength of the source for frequencies of up to 8–33 Hz. It is within 0.25 wavelengths of the source at the dominant 2 Hz spectral peak. Therefore, station L22 sees primarily near-field radiation at all frequencies up to at least 8 Hz. This is also true for the dominant 2 Hz spectral peak at stations CMG and MAR: A distance of 700 m to the farthest station (MAR) places it within one wavelength of the source for the 2 Hz spectral peak. This argument is identically true if the tremor source is the lava lake itself. In this case, station L22 would be even closer to the source.

The insight into possible tremor sources is the following. The near-field radiation pattern of a double-couple source produces radiation in both transverse directions (Aki and Richards, 2002). Because all three stations record primarily near-field seismic waves, and

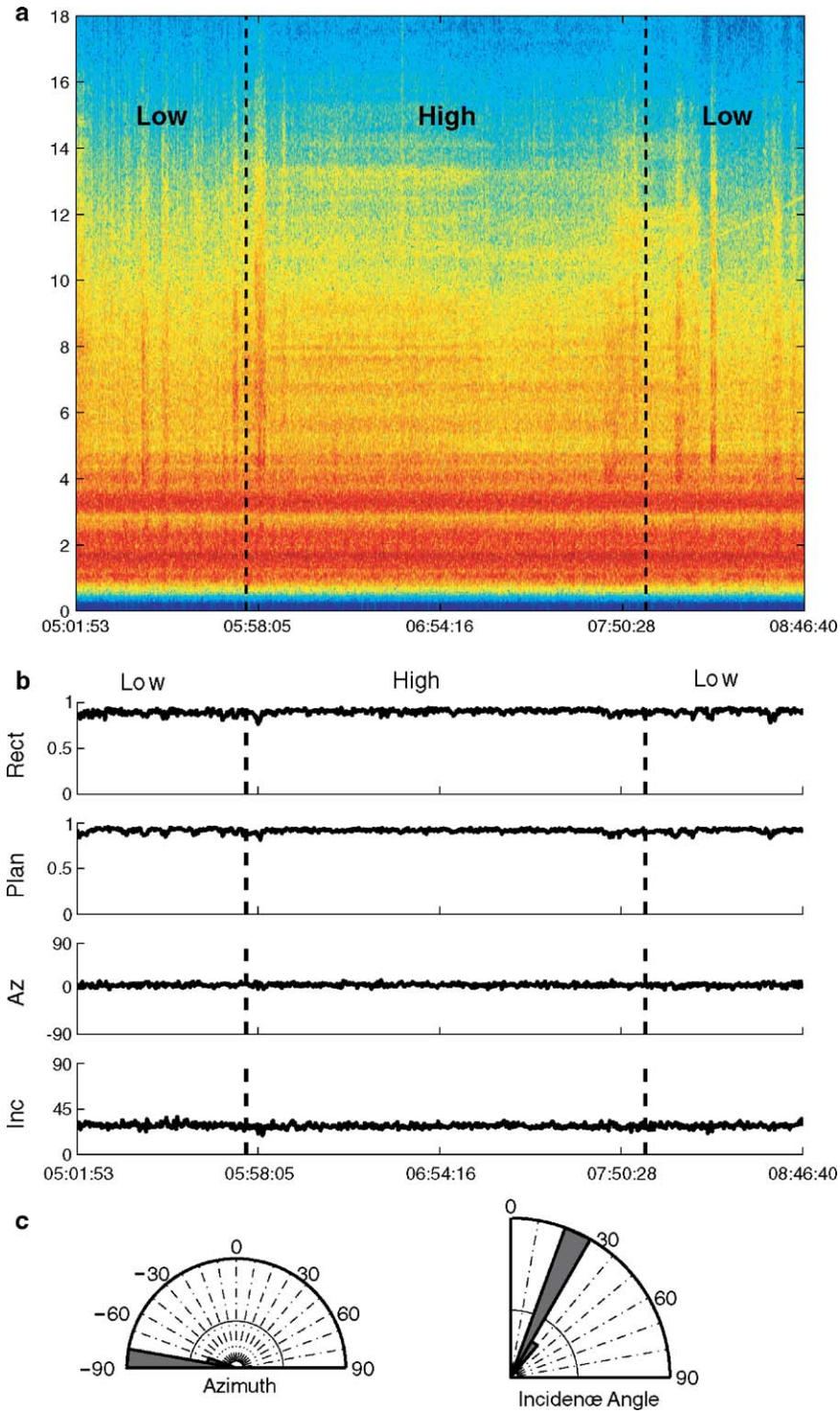

Fig. 4. Spectrogram and polarization of a 3-h 45-min segment of continuous tremor data, recorded at station L22, beginning 19 February 2002, 05:01 GMT. Data are filtered using a two-pass, four-pole Butterworth band pass filter, with corners at 0.8 and 12 Hz. Polarization is computed for non-overlapping, 20-s data segments. (a) Spectrogram. (b) Time series of computed polarization. From top to bottom: plotted time series are azimuth, incidence angle, rectilinearity, and planarity. Convective regimes are labeled “low” and “high”. Approximate transition times are indicated by dotted lines. (c) Rose diagrams showing clustering of azimuth (left) and incidence angle (right).

because the wavefield is radially or almost radially polarized everywhere, double-couple sources for Erta 'Ale's tremor are completely ruled out. One need consider only possible tremor source mechanisms which are capable of producing this radiation pattern. These are limited to an isotropic source or a vertical CLVD.

6. Tremor location

To clarify the ambiguous results of polarization analysis, and to better understand the tremor's physical source process, we next attempt to locate segments of continuous tremor. However, because a maximum of

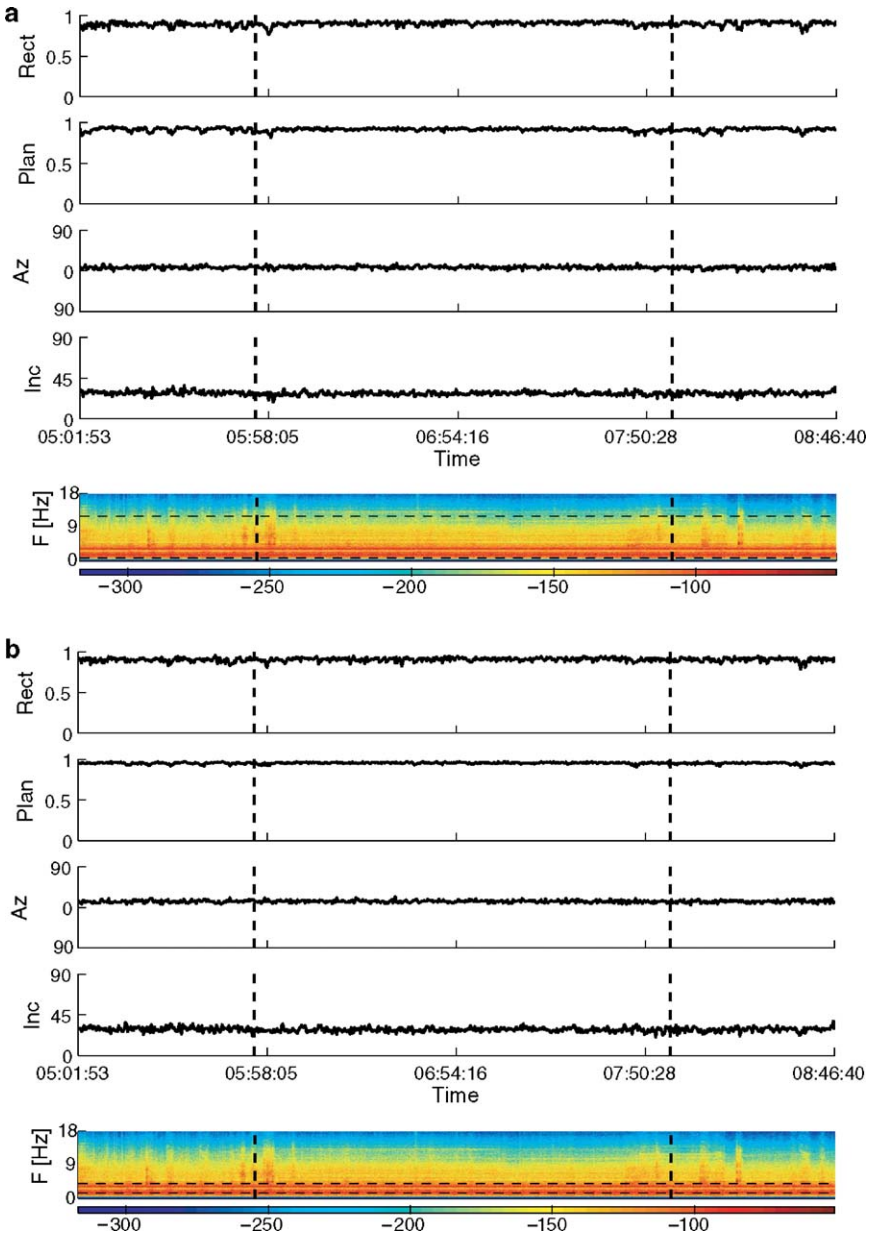

Fig. 5. Polarization analysis for a 3-h 45-min segment of continuous tremor data, recorded at station L22, beginning 19 February 2002, 05:01 GMT. Data are filtered in four narrow, overlapping frequency bands, using a two-pass, four-pole Butterworth band pass filter. Polarization is computed for non-overlapping, 20-s data segments. From top to bottom: plotted time series are azimuth, incidence angle, rectilinearity, and planarity, filtered between (a) 0.8–2 Hz, (b) 1.5–2 Hz, (c) 3.5–6 Hz, and (d) 5.5–12 Hz. The lowermost subplot of each figure is a vertical-component spectrogram from station L22, showing energy between 0 and 18 Hz, with relevant frequencies of each subplot indicated by horizontal dotted lines. Approximate transition time is indicated by a vertical dotted line.

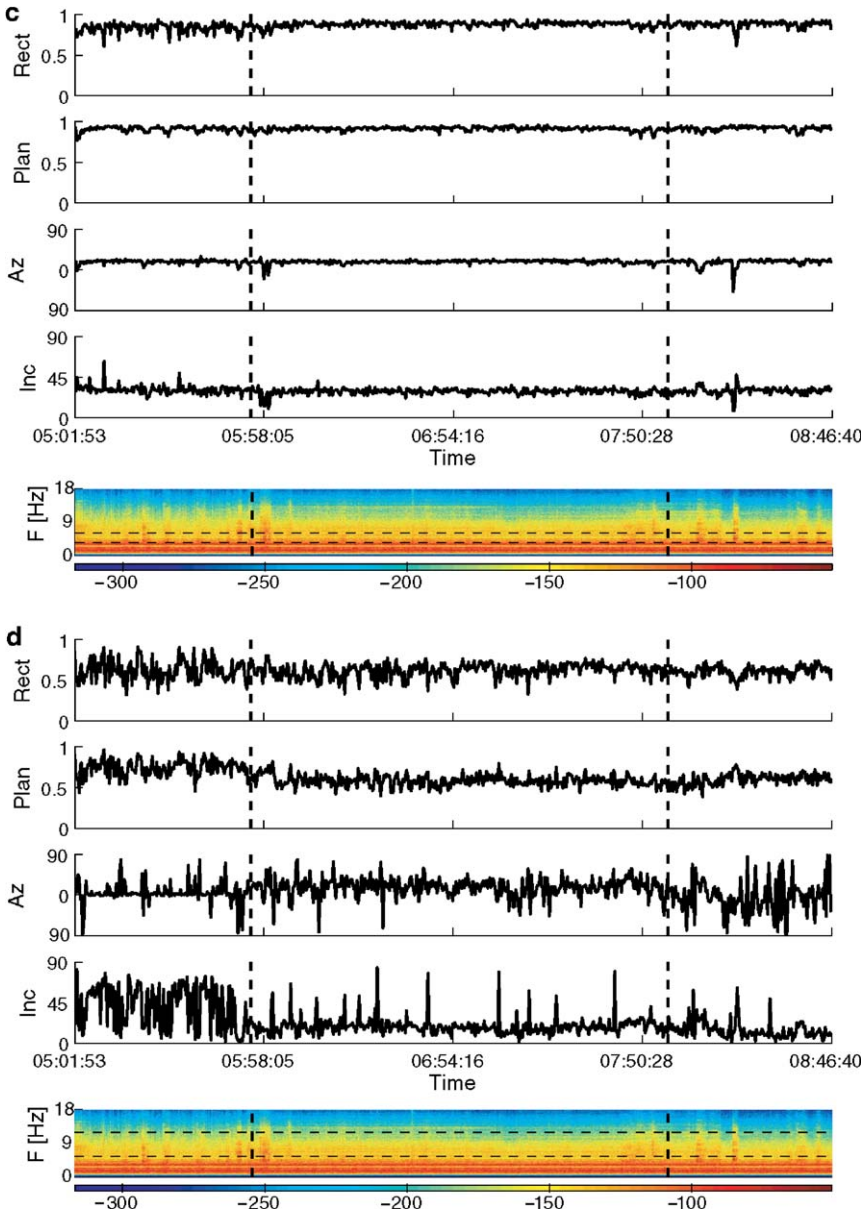

Fig. 5 (*continued*).

three stations were operational at any time, even an epicentral location cannot be treated as correct in an absolute sense: with three stations in a nearly linear configuration, location results are always affected by station geometry. However, two important clues can be gained. First, the scatter in such locations provides a first-order measure of how well tremor can be approximated by a stationary point source. Second, characteristic differences in tremor locations indicate that either the true location or the source mechanism must change. It is this second piece of information which is most important to this study, because we wish primarily to answer the question of which changes in spectral content and polarization – already associated with changes in the lava lake's convective behavior – reflect a changing source location or mechanism.

To locate Erta 'Ale's continuous tremor, we select an amplitude-based method modified from techniques introduced by Gottschämmer and Surono (2000). Because these techniques have successfully located tremor with

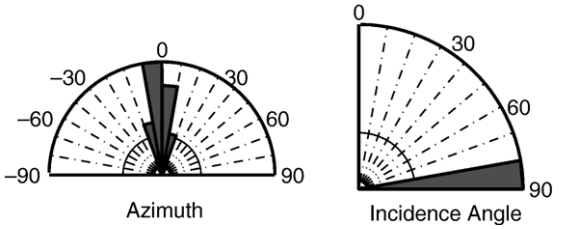

Fig. 6. Rose diagrams of azimuth (left) and incidence angle (right) for a 3-h 45-min segment of continuous tremor data, recorded at station MAR, beginning 19 February 2002, 05:01 GMT. Data are filtered using a two-pass, four-pole Butterworth band pass filter, with corners at 0.8 and 12 Hz. Polarization is computed for non-overlapping, 20-s data segments.

similar amplitude, recorded with similar three-station deployments (Gottschämmer, 1999), and because polarization already suggests an isotropic source, this choice of methods is appropriate. Even if the source is a vertical CLVD, the lack of seismometers directly above it insures that the radiation pattern is very nearly isotropic, and the fundamental assumption of an isotropic source remains valid for purposes of locating the tremor.

We begin by reviewing the basis for their method. Assuming an isotropic source, and adopting their notation, emitted source power will be given by

$$P = 4\pi R^2 \rho v e^{\kappa R} y^2 \tag{1}$$

where y represents the ground velocity, density is ρ, phase velocity is v, absorption coefficient is κ, and distance from the source is R (Gottschämmer and Surono, 2000). Rather than directly using the velocity amplitude y of the signal, which continuously oscillates, one can derive a more stable quantity linked to the envelope of the signal. This is done by substituting y with the average velocity amplitude y, easily calculated from the velocity seismograms, by computing the integral

$$Y(t) = \int_{t_1}^{t_2} y^2 \mathrm{d}t \tag{2}$$

where t_1 and t_2 are the beginning and ending times of a tremor segment. If a signal is stable over time, then one can use identical t_1 and t_2 values at all stations, as the signal envelope should be constant. This is a distinct advantage over methods that assume tremor propagates as a plane wave, as it removes the dependence of results on correctly guessing phase velocity.

The source power can then be calculated from the observed average velocity amplitude y, and an estimated source–receiver distance R. The point whose set of source–receiver distances yields the most nearly isotropic source is the best source location.

While this method appears robust, we find a grid-search technique unsatisfactory for the following reason: fundamental to the grid-search technique, and resultant statistical analysis, is that the effects of scattering and converted phases are neglected. This is particularly problematic in a volcanic environment. Scattering in a highly heterogeneous medium can create an arbitrarily complex wavefield, even at distances of only a few wavelengths from the tremor source. In the case of Erta ‘Ale, if the tremor source is the lava lake itself, this is possible even as close as station MAR (Fig. 2).

Because of this difficulty, and because a grid search method has inherently limited resolution, we adopt a least-squares routine which weights data to account for scattering. This approach is based on the same isotropic source assumption, which considers small perturbations m to a trial source location m_0, and seeks to minimize the residual difference between mean source power, $\bar{P}$, at all seismic stations, and source power P_i at each seismic station, calculated using y and R. Explicitly, the “residual” $r_i(m)$ is defined at each station i as

$$r_i(m) = \bar{P} - P_i(m) \tag{3}$$

Taking the Taylor’s series expansion of this residual gives

$$r_i(m) = r_i(m_0) - \frac{\partial P_i}{\partial m_j}\Delta m_j \tag{4}$$

Thus, we seek corrections to our trial location m_0 such that

$$r_i(m_0) = \frac{\partial P_i}{\partial m_j}\Delta m_j \tag{5}$$

We can therefore form a least-squares problem to invert for corrections to this trial location, using the partial derivatives of isotropic source power with respect to the epicentral coordinates,

$$\frac{\partial P_i}{\partial x} = 4\pi\rho v y^2 x e^{\kappa R}(2+\kappa R)$$

$$\frac{\partial P_i}{\partial y} = 4\pi\rho v y^2 y e^{\kappa R}(2+\kappa R). \tag{6}$$

To properly weight the inversion, it is desirable to introduce an independent measure of each station’s data quality. Since an isotropic source generates only body waves, with strictly rectilinear motion, it is natural to weight data quality using rectilinearity. This has already been calculated, cf. above, by the method of Jurkevics

(1988). The diagonals of our weighting matrix are thus simply the rectilinearity values for each data segment at each station. In this way, if scattered or converted phases feature prominently in station data, the resultant decrease in rectilinearity will penalize that station's data. This is similar to the weighting scheme introduced to semblance methods by Kawakatsu et al. (2000), in that it quantifies the degree to which data at a particular station reflect a purely isotropic source.

Finally, to insure that our inversion uses only the rectilinear part of the signal, the three-component seismic data must be rotated into the azimuth and incidence angle, as calculated from polarization analysis. In this way, the Z' component measures only motion toward and away from the source, and can be used to calculate the average velocity amplitude, y.

It remains to quantify the error associated with this inversion. This requires three assumptions. If we assume uncertainties are approximately the same at each station, and that data errors are statistically independent, and that tremor source size is exactly known, then the covariance matrix of the least squares solution (Menke, 1989) reduces to:

$$\left[mm^T\right] = \left[A^T A\right]^{-1}\sigma^2 I \tag{7}$$

where σ^2 is the solution variance, A is the matrix of partial derivatives in Eq. (6), and I is the 2×2 identity matrix. The diagonals of this covariance matrix give the error estimate for each model parameter, x and y.

For each station, we calculate the partial derivatives (Eq. (6)) based on calculated average velocity amplitude, y, a density of 2.7 kg/m^3, and a phase velocity of 2.2 km/s. The trial location m_0 is 10 m north of the station whose average velocity amplitude (Eq. (2)) is greatest. Final locations are determined from six iterations of the inversion routine. Because the directly measured quantity is average velocity amplitude y, and density and phase velocity are assumed to be uniform everywhere, absolute errors in density or phase velocity affect computed source power, but not the location itself.

Locations were produced for all time periods with three stations operational for more than 10 min. In this way, we analyzed two time windows from the high convective phase and six windows from the low convective phase. Table 2 shows specific time periods and window lengths used. We computed locations for each available segment of data from each convective regime, then analyzed one representative sample of each regime in detail.

7. Results and discussion

The epicenters of all locatable tremor segments are plotted in Fig. 7. Light circles represent tremor from the low convective regime; dark circles represent tremor from the high convective regime. Location errors are not visible because they are smaller than the points themselves. It is immediately clear that tremor from each convective regime locates to a unique region; that both regions lie within the three-station network; that tremor from each convective regime is consistent with body-wave azimuths from all stations; and that the two regions are sufficiently close that polarization analysis alone cannot completely resolve location differences. Computed source power is different between the two convective phases, measuring 59 W during the high convective phase, and 38–42 W during the low convective phase (Table 2). This suggests that these locations may represent the true positions of tremor epicenters, and that tremor is not generated in the lava lake itself. Such a finding is somewhat counterintuitive, and requires more investigation. Therefore, to test in detail the stability of these tremor locations, and to verify this finding, we analyze one representative sample from each convective regime, computing locations in short, non-overlapping segments.

For the detailed analysis, a segment length of 20 s is chosen to characterize the spatial extent of tremor

Table 2
Analyzed tremor samples

Start Time (mm/dd hh:mm:ss)	Length (s)	Convective regime	Power (W)	Latitude	Longitude	Incidence angle (°)	Depth (m asl)	Notes
02/15 16:28:45	1168	Low	37.24	13.603408	40.665340	28.02	109	
02/15 16:53:20	843	Low	40.83	13.603283	40.665286	28.00	111	
02/15 17:23:19	821	Low	39.93	13.603302	40.665309	28.10	109	
02/15 17:43:19	1137	Low	38.44	13.603341	40.665263	28.35	125	Fig. 8
02/15 18:03:19	674	Low	42.36	13.603236	40.665244	27.56	107	
02/15 19:33:20	756	High	59.65	13.602779	40.665024	29.38	126	
02/15 19:53:21	1033	High	59.17	13.602699	40.665074	31.82	146	Fig. 9
02/15 22:13:20	695	Low	38.95	13.603298	40.665414	38.49	228	

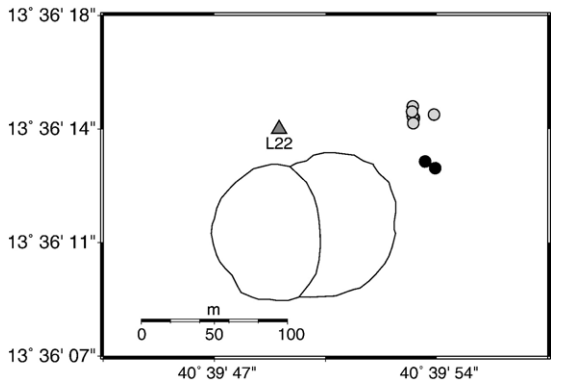

Fig. 7. Locations of all tremor data samples longer than 10 min. Light circles represent tremor from the low convective regime; dark circles represent tremor from the high convective regime. Location errors are not visible because they are smaller than the points themselves. Seismic stations are indicated with labeled triangles. A scale is provided at lower left.

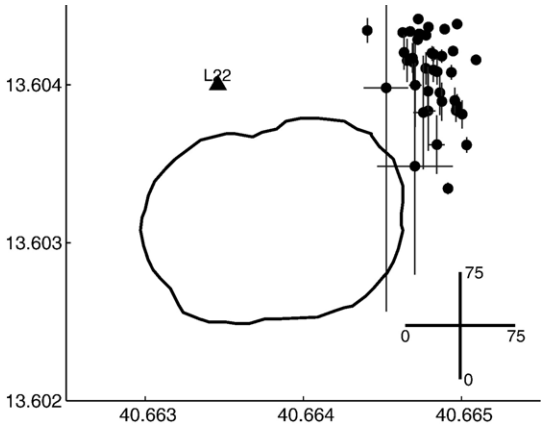

Fig. 8. Locations for a sample data window recorded during the low convective regime. Tremor is located in non-overlapping, 20 s segments. Sample window begins 15 February 2002, 17:43 GMT, and lasts approx. 19 min. Error bars in the x and y directions are plotted using solid lines that underlie each point. Seismic stations are indicated with labeled triangles. Scale is plotted at lower right.

epicenters. Longer location window lengths, of course, produce less scatter, as they are less sensitive to data glitches and transients (e.g. rock falls), and will have smaller location errors. On the other hand, using a shorter time window shows an inherent location scatter which error analysis alone cannot.

Results of this detailed analysis appear in Figs. 8 and 9. During the low convective phase, continuous tremor locates predominantly E of station L22 (Fig. 8), in a region 200 m long by 100 m wide. Calculated source power remains relatively stable at 31–48 W. During the high convective phase, continuous tremor locates E to ESE of station L22 (Fig. 9), but some segments partially overlap tremor locations of the low convective phase (Fig. 8). Calculated power fluctuates between 50 and 65 W. We note that the best locations from each detailed sample, i.e. those whose errors are smallest, generally do not overlap. These locations are excellent for both convective regimes; no error bars are visible for many individual tremor segments, because they are smaller than the points themselves ($\sigma \sim 10^{-2}$–10^{-4} m). Since these shorter tremor segments have epicenters consistent with those of longer segments, and many of these shorter segments do not overlap, we conclude that differences in tremor location are not simply a result of long-term averaging.

Although tremor source depth cannot be constrained with only three seismic stations, we can place a first-order constraint on tremor depths using trigonometry, incidence angles, and epicentral distances. Because station L22 is closest to the tremor epicenters of Fig. 7, and rectilinearity at this station takes values of >0.90, this station best represents the source properties of the seismic wavefield. We therefore tabulate incidence angles at station L22, and use these calculate approximate source depths, in Table 2. We find that estimated tremor depth is generally stable for both regimes at 110–150 m asl, or 310–360 m below the lava lake surface.

Finally, we discuss the robustness of tremor locations using a simple robustness test, wherein one station's data is multiplied by a constant before a location is computed. The constant varies from 0.3 to 3.0 in increments of 0.1. In this way, the location is tested for stability to amplification of each station's seismic sig-

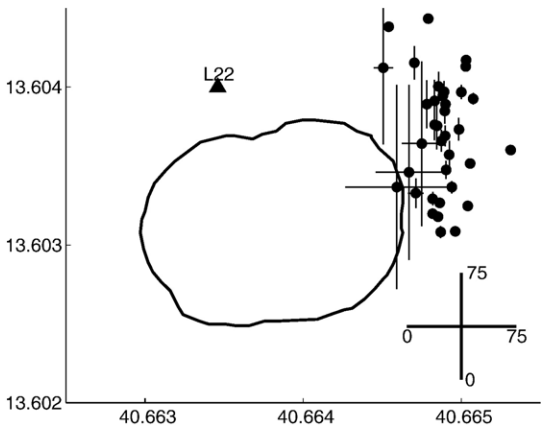

Fig. 9. Locations for a sample data window recorded during the high convective regime. Tremor is located in non-overlapping, 20-s segments. Sample window begins 15 February 2002, 19:53 GMT, and lasts approx. 18 min. Error bars in the x and y directions are plotted using solid lines that underlie each point. Location method is discussed in the text. Seismic stations are indicated with labeled triangles. Scale is plotted at lower right.

nals. Results of this test are shown in Fig. 10. The segment selected for testing is the same as in Fig. 8. From this, we see that the result is affected negligibly by amplifications of station L22, and is more sensitive to amplifications at stations CMG and MAR. We now discuss this result in the context of possible physical causes of site amplification.

There are two ways in which site effects can skew tremor locations computed by this method: A laterally heterogeneous medium, and amplification of seismic waves by surface geology. We can immediately exclude the former. From Eq. (6) and the definition of P wave velocity (e.g. Aki and Richards, 2002), it follows that ρ must vary laterally by a factor of at least four to affect locations. This is an improbable scenario even in the most heterogeneous volcanic environment.

The possibility remains that site geology can amplify seismic waves, and thereby affect locations. Unfortunately, because no regional earthquakes or teleseisms were recorded above the background tremor, site response cannot be estimated. Further, rectilinearity values are not high enough at stations MAR and CMG to rule out the possibility that part of the tremor there is composed of scattered Rayleigh waves. Thus, even approximate methods of estimating site response (e.g. Nakamura, 1989) are inapplicable. However, stations L22 and MAR are installed in structurally similar regions of the active crater (compare Fig. 2 to Oppenheimer and Francis, 1998 and Fig. 2 to Tazieff, 1984). Thus the likeliest candidate for geologic site effects is station CMG. Because locations are robust to site amplifications of 0.5–2.0 at station at CMG (Fig. 10), and are similarly robust at station MAR, site amplification must be outside this range to significantly affect locations. Although such an amplification factor is possible in some volcanic environments, the similar surface geology at these sites, and the absence of sediment and ash deposits, make this an unlikely possibility.

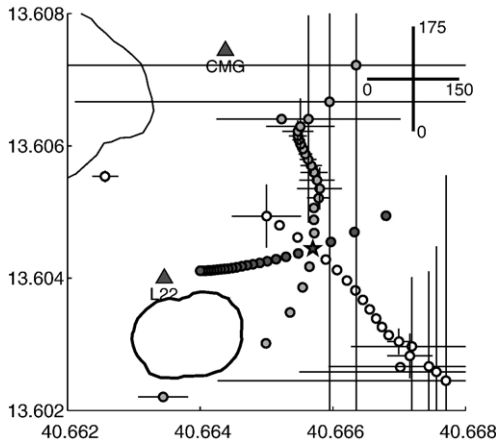

Fig. 10. Robustness test for a 19-min sample data window beginning 15 February 2002, 17:43 GMT. Gray star represents the location computed with no introduced amplification factor. Each series of circles represents multiplication of data from one station by one constant prior to location, with circles nearer to the test location representing gains close to 1.0, and circles farther away representing larger (or smaller) amplifications. Dark gray circles correspond to amplification of station L22 data; light gray circles correspond to station CMG; white circles correspond to station MAR. Thick solid line indicates approximate position of active crater. Thin solid line indicates approximate position of extinct north crater. Scale is shown at upper right. Triangles represent seismic stations. Station MAR is shown in Fig. 2.

The robustness test of Fig. 10 confirms two important clues about the tremor source. First, the locations shown in Fig. 7 are robust to reasonable site amplifications. Second, no reasonable site amplification factor both gives a convergent solution to the location problem, and places the location underneath the lava lake.

8. Implications for tremor source process

Because spectral content, polarization, and epicentral location all change between convective phases, and these changes are consistent with changes in thermal data, it follows that convection directly affects the volcanic tremor, even if tremor does not originate in the active lava lake. It remains to discuss what possible source processes could generate the tremor, and, further, what physical changes are required in the magma system at Erta ‘Ale to produce tremor at the computed locations, with the observed polarizations.

We cannot uniquely determine the tremor source mechanism from these data alone, but several models can be ruled out, and a conceptual model can be developed based on our observations. The stable polarization and frequency content of each convective phase argue against destructive source mechanisms for either convective regime. Displacement of a fluid-filled crack (e.g. Chouet, 1986, 1988) is also excluded, because the tremor’s spectral content is not harmonic. We prefer models wherein some near-surface gas process generates the tremor. Because a steady supply of fresh, gas-rich magma must balance heat lost from the lava lake surface (Harris et al., 1999), gas-driven processes account for the unchanging spectral characteristics of tremor from each convective regime.

It must be noted, however, that this does not completely explain observed differences in spectral content (and locations) for the two convective regimes. We explain these using a conceptual model of the variable

convection, based on our model in Harris et al. (2005). As the surface of the active lava lake cools, it forms a viscous, slow-moving layer. As this layer degasses, density and viscosity increase, and gas pressurizes in a conduit. This buildup is expressed in the form of gas bubble coalescence, in a conduit some 300–350 m below the lava lake surface, which radiates isotropically as tremor (Ripepe and Gordeev, 1999). This conceptually explains tremor in the 0.8–6 Hz range, which persists at all times with relatively constant energy (Fig. 3).

Eventually, when convective overturn is triggered, the thin, crusted surface cracks, allowing trapped gases to escape. The combination of cracking crust and sinking cooled, viscous magma generates the high frequency energy, which is superimposed as a second, broadband (6–12 Hz) tremor signal. Because the lower frequency background tremor always dominates the signal (Fig. 3), the superimposed high-frequency signal cannot completely shift tremor locations to the lava lake. Instead locations are perturbed by a small amount due to the contribution of this second tremor source.

Unfortunately, this source mechanism cannot be tested further in a quantitative way. Filtering tremor at 6–12 Hz and computing locations for the high regime will not necessarily produce accurate results. Even at 6 Hz, the seismograms of station L22 would primarily consist of near field, isotropic seismic radiation, but could include scattered waves at CMG and MAR. This would not greatly affect locations of tremor in a wider frequency band, because the dominant 2 Hz frequency contains most of the energy, and will most affect computed source power. However, while this only causes a slight increase in computational error at low frequencies, restricting our analysis to only a higher frequency band means that the location method's fundamental assumptions (isotropic source, radial polarization) do not necessarily apply.

Our model for low-frequency tremor is similar to experimental work by Jaupart and Vergnoille (1988), involving coalescence and subsequent bursting of gas bubbles. It also has some similarities to the model proposed by Rymer et al. (1998) for shallow conduit convection at Masaya, Nicaragua, where anomalous gas release was associated with convective overturn of magma in a shallow conduit, followed by steady degassing. The time scales are much shorter for this proposed model at Erta 'Ale than for Masaya, but it should be noted that these time scales are appropriate for the more rapid convection at Erta 'Ale.

On the other hand, our conceptual model differs substantially from tremor models at other basaltic volcanoes, including some scenarios for Stromboli (e.g. Chouet et al., 1997). In this model, for instance, a foam could accumulate below the lava lake surface, and, rather than forming gas slugs, simply rupture the surface, generating a seismic wavefield. The polarization of Erta 'Ale tremor argues against propagation of gas slugs in the underlying conduit, as the resultant conduit resonance would produce incidence angles scattered over the conduit's height. On the contrary, we find that incidence angles are relatively stable (Figs. 4 and 6 and Table 2). Further evidence against the foam/gas slug model comes from the lack of vigorous fountaining and Strombolian blasts at Erta 'Ale. As for Stromboli (Ripepe and Gordeev, 1999; Ripepe et al., 2002), the inclusion of an infrasonic and gas flux data set, and the study of the temporal evolution of the interaction between seismic, infrasonic, gas flux, and thermal data, could shed more light on the tremor generation process.

9. Conclusions

After decades of restricted or impossible access, field campaigns can once again study magma convection and its associated signals at the extraordinarily longstanding Erta 'Ale lava lake. Seismic, thermal, and video data show that lava lake convection is not constant, but instead cycles between two regimes characterized by low (0.01–0.08 m s^{-1}) and high (0.1–0.4 m s^{-1}) surface velocities, on time scales of tens to hundreds of minutes. Tremor polarization and location suggests a shallow, nondestructive, volumetric tremor source. We propose a conceptual model wherein bubble coalescence in a conduit generates the observed lower frequency (0.8–6 Hz tremor), and that the upper end of this conduit is the lava lake. As convective overturn is triggered in the lava lake, the combination of cracking lava lake crust, gas escape, fountaining, and sinking degassed magma generates the higher-frequency signal (6–12 Hz), which characterizes the high convective regime.

It must be noted that even if the location shift observed in Figs. 7–9 can be ascribed to an added, secondary tremor source, there must exist some tremor source mechanism responsible for an apparent location change during the high convective regime. This is important, because it shows that amplitude-based location techniques can detect changes that relate directly to behavior of at least this one volcano.

The convective regimes of Erta 'Ale are similar to the variable degassing regimes at Stromboli volcano, Italy, reported by Ripepe et al. (2002), and suggest a tremor source mechanism similar to that proposed by Ripepe and Gordeev (1999). However, in the case of

Erta ‘Ale, variability in the spectral content of tremor can be explained entirely in terms of processes taking place in the shallower part of the system, such as cooling and degassing (Harris et al., 2005). Similarities to the model of Rymer et al. (1998) for Masaya, Nicaragua, and the model of Ripepe and Gordeev (1999) for Stromboli, the suggest that the convective behavior observed at Erta ‘Ale, and its associated tremor, may be expressions of a general model for shallow convection at persistently active basaltic volcanoes.

Acknowledgements

We thank OGS–CRS, Udine (Italy) for providing seismic station MAR, the PNSN, Seattle (WA) for seismic station CMG and the DAS for station L22, and Tom Yelin (USGS, Seattle, WA) for generous loan of the L22 sensor. The expedition benefited from logistical support by the Afar Government and Geo-Decourverte. J. Alean, M. Fulle and the rest of the group were invaluable companions in the field. E. Gottschämmer and M. Di Cecca shared software with us. R. Carniel was funded by MULTIMO project (Energy, Environment and Sustainable Development Program, EU Contract no. EVG1-CT-2000-00021). AJLH was funded by NSF grant EAR-0106349. J. Jones is thankful for funding contributions from Ms. Deborah A. Freed. We thank our anonymous reviewers for their suggestions, which have hopefully led to significant improvements of this paper.

References

Aki, K., Richards, P.G., 2002. Quantitative Seismology (Second Edition). Published by University Science Books, Sausalito, CA, 700 pp.

Alean, J., Carniel, R., Fulle, M., 2005. Stromboli online – volcanoes of the world: Information on Stromboli, Etna and other volcanoes. http://stromboli.net.

Amelung, F., Oppenheimer, C., Segall, P., Zebker, H., 2000. Ground deformation near Gada ‘Ale Volcano, Afar, observed by radar interferometry. Geophys. Res. Lett. 27 (19), 3093–3096.

Aspinall, W.P., Woo, G., Voight, B., Baxter, J., 2003. Evidence-based volcanology: application to eruption crises. J. Volcanol. Geotherm. Res. 128, 273–285.

Aspinall, W.P., Carniel, R., Jaquet, O., Woo, G., Hincks, T., 2006. Using hidden multi-state Markov models with multi-parameter volcanic data to provide empirical evidence for alert level decision-support. J. Volcanol. Geotherm. Res. 153, 112–124. doi:10.1016/j.jvolgeores.2005.08.010.

Aster, R., McIntosh, W., Kyle, P., Esser, R., Bartel, B., Dunbar, N., Johns, B., Johnson, J., Karstens, R., Curnik, C., McGowan, N., McNamara, S., Meertens, C., Pauly, B., Richmond, M., Ruiz, M., 2004. Real-time data received from Mount Erebus Volcano, Antarctica. Eos Trans. AGU 85 (10), 97–100.

Barberi, F., Varet, J., 1970. The Erta ‘Ale volcanic range. Bull. Volcanol. 34, 848–917.

Barker, S.R., Sherrod, D.R., Lisowski, M., Heliker, C., Nakata, J.S., 2003. Correlation between lava-pond drainback, seismicity, and ground deformation at Pu‘ u O‘ O. U.S. Geol. Surv. Prof. Pap. 1676, 53–62.

Carniel, R., Di Cecca, M., Rouland, D., 2003. Ambrym, Vanuatu (July–August 2000): spectral and dynamical transitions on the hours-to-days timescale. J. Volcanol. Geotherm. Res. 128, 1–13.

Carniel, R., Di Cecca, M., Jaquet, O., 2006. A user-friendly, dynamic web environment for remote data browsing and analysis of multi-parametric geophysical data within the MULTIMO project. J. Volcanol. Geotherm. Res. 153, 80–96. doi:10.1016/j.jvolgeores.2005.08.005.

Chouet, B.A., 1986. Dynamics of a fluid-driven crack in three dimensions by the finite difference method. J. Geophys. Res. 91, 13967–13992.

Chouet, B.A., 1988. Resonance of a fluid-driven crack: radiation properties and implications for the source of long-period events and harmonic tremor. J. Geophys. Res. 93, 4375–4400.

Chouet, B.A., Saccorotti, G., Martini, M., Dawson, P., De Luca, G., Milana, G., Scarpa, R., 1997. Source and path effects in the wave fields of tremor and explosions at Stromboli volcano, Italy. J. Geophys. Res. 102 (B7), 15129–15150.

Dainelli, G., Marinelli, O., 1907. Vulcani attivi della Dancalia. Riv. Geogr. Ital. 13, 261–270.

Duffield, W.A., 1972. A naturally occurring model of global plate tectonics. J. Geophys. Res. 77 (14), 2543–2555.

Francis, P.W., Oppenheimer, C., Stevenson, D., 1993. Endogenous growth of persistently active volcanoes. Nature 366, 554–557.

Gottschämmer, E., 1999. Volcanic tremor associated to volcanic activity at Bromo Volcano. Ann. Geofis. 42, 465–481.

Gottschämmer, E., Surono, I., 2000. Locating tremor and shock sources at Bromo Volcano. J. Volcanol. Geotherm. Res. 101, 199–209.

Hamaguchi, H., Nishimura, T., Zana, N., 1992. Process of the 1977 Nyiragongo eruption inferred from the analysis of long-period earthquakes and volcanic tremors. Tectonophysics 209, 241–254.

Hantke, G., 1939. Ubersicht uber die Vulkanische Tatigkeit vom Januar 1937 bis Marz 1938. Zeit. Deut. Geol. Ges. 91, 160–168.

Harris, A.J.L., Flynn, L.P., Rothery, D.A., Oppenheimer, C., Sherman, S.B., 1999. Mass flux measurements at active lava lakes: implications for magma recycling. J. Geophys. Res. 104 (B4), 7117–7136.

Harris, A.J.L., Carniel, R., Jones, J., 2005. Identification of variable convective regimes at Erta Ale Lava Lake. J. Volcanol. Geotherm. Res. 142, 207–223.

Jaupart, C., Vergnoille, S., 1988. Laboratory models of Hawaiian and Strombolian eruptions. Nature 331, 58–60.

Jurkevics, 1988. Polarization analysis of three-component array data. Bull. Seismol. Soc. Am. 78, 1725–1743.

Kaminuma, K., 1994. The seismic activity of Mount Erebus in 1981–1990. AGU Antarct. Res. Ser. 66, 35–50.

Kawakatsu, H., Kaneshima, S., Matsubayashi, H., Ohminato, T., Sudo, Y., Tsutsui, T., Uhira, K., Yamasato, H., Ito, H., Legrand, D., 2000. Aso94: aso seismic observation with broadband instruments. J. Volcanol. Geotherm. Res. 101, 129–154.

Kyle, P.R., 1994. Volcanological and environmental studies of Mount Erebus, Antarctica. AGU Antarct. Res. Ser. 66, 162 pp.

Kyle, P.R., Sybeldon, L.M., McIntosh, W.C., Meeker, K., 1994. Sulfur dioxide emission rates from Mount Erebus, Antarctica. AGU Antarct. Res. Ser. 66, 69–82.

Lachlan-Cope, T., Smellie, J.L., Ladkin, R., 2001. Discovery of a recurrent lava lake on Saunders Island (South Sandwich Islands) using AVHRR imagery. J. Volcanol. Geotherm. Res. 112, 105–116.

Le Guern, F., 1987. Mechanism of energy transfer in the lava lake of Nyiragongo (Zaire), 1959–1977. J. Volcanol. Geotherm. Res. 31, 17–31.

Macdonald, G.A., Abbott, A.T., Peterson, F.L., 1970. Volcanoes in the Sea. Univ. Hawai'i Press, Honolulu, HI, 517 pp.

Martini, M., 1969. Studio di prodotti fumarolici di alcuni vulcani della catena dell'Erta Ale (Ethiopia). Rend. Soc. Mineral. Ital. 25, 79–92.

McNutt, S.R., Rymer, H., Stix, J., 2000. Synthesis of volcano monitoring. In: Sigurdsson, H., Houghton, B.F., McNutt, S.R., Rymer, H., Stix, J. (Eds.), Encyclopedia of Volcanoes. Academic Press, San Diego, pp. 1165–1183.

Menke, W., 1989. Geophysical Data Analysis: Discrete Inverse Theory. Academic Press, 289 pp.

Nakamura, Y., 1989. A method for dynamic characteristics estimation of subsurface using microtremor on the ground surface. Q. Rep. RTRI 30 (1), 25–33.

Neuberg, J.W., Tuffen, H., Collier, L., Green, D., Powell, T., Dingwell, D., 2006. The trigger mechanism of low-frequency earthquakes on Montserrat. J. Volcanol. Geotherm. Res. 153, 37–50. doi:10.1016/j.jvolgeores.2005.08.008.

Oppenheimer, C., Francis, P., 1997. Remote sensing of heat, lava and fumarole emissions from Erta 'Ale volcano, Ethiopia. Int. J. Remote Sens. 18, 1661–1692.

Oppenheimer, C., Francis, P., 1998. Implications of longeval lava lakes for geomorphological and plutonic processes at Erta 'Ale volcano, north Afar. J. Volcanol. Geotherm. Res. 80, 101–111.

Patrick, M.P., Smellie, J.L., Harris, A.J.L., Garbeil, H., Pilger, E., 2005. First recorded eruption of Mount Belinda volcano, South Sandwich Islands. Bull. Volcanol. 67, 415–422.

Ripepe, M., Gordeev, E., 1999. Gas bubble dynamics model for shallow volcanic tremor at Stromboli. J. Geophys. Res. 104 (B5), 10639–10654.

Ripepe, M., Harris, A.J.L., Carniel, R., 2002. Thermal, seismic and infrasonic evidences of variable degassing rates at Stromboli volcano. J. Volcanol. Geotherm. Res. 118, 207–285.

Rymer, H., van Wyk de Vries, B., Stix, J., Williams-Jones, G., 1998. Pit crater structure and processes governing persistent activity at Masaya Volcano, Nicaragua. Bull. Volcanol. 59, 345–355.

Swanson, D.A., Duffield, W.A., Jackson, D.B., Peterson, D.W., 1979. Chronological narrative of the 1969–71 Mauna Ulu eruption of Kilauea volcano, Hawaii. U.S. Geol. Surv. Prof. Pap. 1056, 55 pp.

Tazieff, H., 1977. An exceptional eruption: Mt Nyiragongo, Jan 10th, 1977. Bull. Volcanol. 40, 189–200.

Tazieff, H., 1984. Mt. Nyiragongo: renewed activity of the lava lake. J. Volcanol. Geotherm. Res. 20, 267–280.

Tazieff, H., 1994. Permanent lava lakes – observed facts and induced mechanisms. J. Volcanol. Geotherm. Res. 63, 3–11.

Tilling, R.I., 1987. Fluctuations in surface height of active lava lakes during 1972–71 Mauna Ulu eruption, Kilauea Volcano, Hawaii. J. Geophys. Res. 92 (B13), 13721–13730.

Witter, J.B., 2003. Convection of magma in volcanic conduits as a degassing mechanism at active volcanoes. PhD thesis, Univ. Washington, Seattle, WA, USA.